Intermediate Phase In-situ Self-reconstruction of Amorphous NASICON for Long-life Solid-state Sodium Metal Batteries

Benben Wei[a], Shuo Huang[a], Xuan Wang[a], Min Liu[b], Can Huang[a], Ruoqing Liu[a], Hongyun Jin[a]*

a. Engineering Research Center of Nano-Geomaterials of Ministry of Education, Faculty of Materials Science and Chemistry, China University of Geosciences, Wuhan 430074, China

b. HYLi Create Energy Technology Co., Ltd, Suzhou 215000, China

Experimental Section

Preparation of NASICON-type electrolyte pellets: All the electrolytes were synthesized and sintered into ceramic pellets through traditional solid-state method. Na_2CO_3, ZrO_2, SiO_2 and $NH_4H_2PO_4$ were mixed by ball-milling with isopropanol at 450 rpm for 12h in a stoichiometric ratio. 10wt.% excess of Na_2CO_3 was added to compensate the sodium volatilization during high temperature calcining process. The dried mixture was calcined at 1000°C for 12 h in air to obtain precursor ceramic, with a temperature ramp-up rate of 5°C min^{-1}. The obtained ceramic powder was manually ground using a mortar and pestle, and further refined by ball milling at 450 rpm for 12 h. Then 0.3g obtained powder was pressed into green pellets (diameter of 12 mm, thickness of 1.2 mm) through isostatic pressing at 8 MPa. Finally, the pellets were calcined at 1250°C for 24h with temperature increasing rate of 2°C min^{-1}. Extra mother powders were placed both underneath and on top of the pressed pellet. For simplification, the $Na_3Zr_2Si_2PO_{12}$, $Na_{3.1}Zr_2Si_{2.1}P_{0.9}O_{12}$, $Na_{3.2}Zr_2Si_{2.2}P_{0.8}O_{12}$, and $Na_{3.3}Zr_2Si_{2.3}P_{0.7}O_{12}$ are named as NZSP, NZSP-2.1, ISA-NZSP and NZSP-2.3, respectively. ISA-NZSP-1100 was also prepared within the same procedure expect the first synthesis temperature of 1100°C.

Materials Characterization: X-ray diffraction analysis (XRD) was conducted using a bruker D8 Advanced X-ray diffraction analyzer (Cu Kα, λ = 0.154056 nm). X-ray photoelectron spectroscopy (XPS, Thermo SCIENTIFIC ESCALAB Xi^+ ESCAlab250) technology was applied to analyze the chemical information of the ceramic pellets and Na/SSE interface. The depth-profiling XPS analysis was conducted with Ar^+ sputtering. Scanning electron microscope (SEM) images were obtained using a Sigma 300 field emission SEM instrument with energy-dispersive X-ray spectroscopy (EDS). The high-resolution transmission electron microscopy (HRTEM), high-angle annular dark-field scanning transmission electron microscopy (HAADF-STEM), and energy dispersive spectroscopy (EDS) experiments were performed using an FEI Talos F200X G2 microscope equipped with Bruker windowless EDX detector at an accelerating voltage of 200 KV.

Electrochemical Measurements: Ionic conductivity was measured using AC impedance analysis (Zahner). The frequency applied ranged from 10 MHz to 1 Hz with an amplitude of 10 mV. A thin layer of Au was sputtered on each surface of the pellets as blocking electrodes. Ionic conductivity was calculated based on the following Equation: σ = L/(R*S), where σ, L, S, and R represent the ionic conductivity, thickness of electrolyte pellets, electrolyte pellet surface area, and resistance value. Activation energies were calculated from the slope of the resulting Arrhenius plot. The CCD value was evaluated by assembling Na| NASICON| Na symmetric cell using an automatic battery tester system (Land, CT-3001A) at room temperature, which was tested by rate cycling under an initial current density of 0.05 mA cm^{-2} with an increasing step of 0.05 mA cm^{-2}. Na metal foils were directly placed on both sides of the solid electrolyte disc without any post-treatment. The pressure of the hydraulic crimping machine when assembling the coin cell was 800 PSI. Galvanostatic stripping-plating of the Na| NASICON| Na symmetric cells was recorded at room temperature with a current density of 0.1 and 0.3 mA cm^{-2}. The cathode was prepared by thoroughly mixing $Na_3V_2(PO_4)_3$ (70 wt%), Super P (20%), and PVDF (10%) to

form a well-distributed slurry and then it was coated onto Al foil with the active materials loading of 1.3-1.5 mg cm^{-2}. CR2032-typed solid-state sodium metal batteries were assembled by using $Na_3V_2(PO_4)_3$ composite as the cathode with diameter of 8 mm, Na foil as the anode with diameter of 9 mm, NZSP/ISA-NZSP as the solid electrolyte. To wetting the cathode and keeping the nano-flammable property, 5 uL ionic liquid electrolyte (1 M Sodium Bis(fluorosulfonyl)imide in 1-Methyl-1-propylpiperidinium Bis(fluorosulfonyl)imide) was dipped at electrolyte/cathode interface. The full cells were galvanostatically charged/discharged on a Land CT-3001A system at different rates (1C = 117.6 mA g^{-1}), and the cutoff voltage window was set as 2.2-3.8 V. All the assemble process was operated in Ar-filled glovebox and all the electrochemical test was carried out at room temperature.

Calculation Method: Our density functional theory (DFT) calculations[1,2] were carried out in the Vienna ab initio simulation package (VASP) based on the plane-wave basis sets with the projector augmented-wave method[3,4]. The exchange-correlation potential was treated by using a generalized gradient approximation (GGA) with the Perdew-Burke-Ernzerhof (PBE) parametrization[5]. The van der Waals correction of Grimme's DFT-D3 model was also adopted[6]. The energy cutoff was set to be 520 eV. The Brillouin-zone integration was sampled with a Γ-centered Monkhorst-Pack mesh of 1 × 1 × 1[7]. The structures were fully relaxed until the maximum force on each atom was less than 0.01 eV/Å, and the energy convergent standard was 10^{-5} eV. The structure was fully relaxed and reached the minimum energy principle during the structure optimization process.

The energy of interface formation (E_{if}) can be calculated using the following equation:

$$E_{if} = [E_{total} - E_{sub1} - E_{sub2}]/\Delta_{interface-area}$$

where E_{total}, E_{sub1}, and E_{sub2} denote the energy of the optimized interfacial system, the substrate Na (110) slab model, and the substrate Monoclinal(020)/

rhombohedral(116)/amorphous slab model, respectively. $\Delta_{interface-area}$ means the interfacial area (in unite of Å^2).

The amorphous structure is simulated by ab initio molecular dynamics simulations (AIMD). The systems are equilibrated at 600K for 5ps and gradually dropped to 300K with a period of another 2ps under an NPT thermostat at ambient pressure.

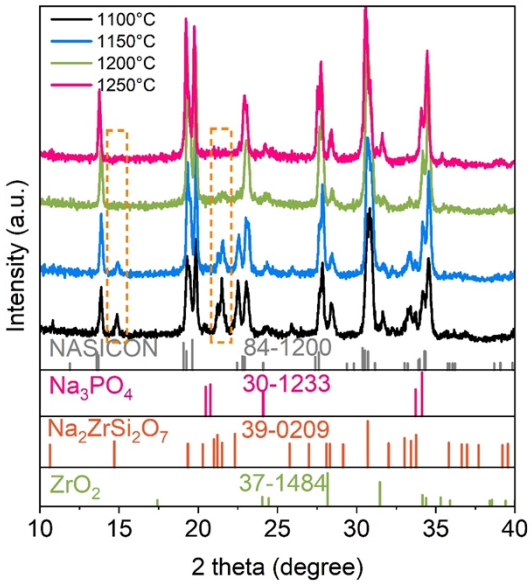

Figure S1. XRD patterns of ISA-NZSP pellets in the sintering process.

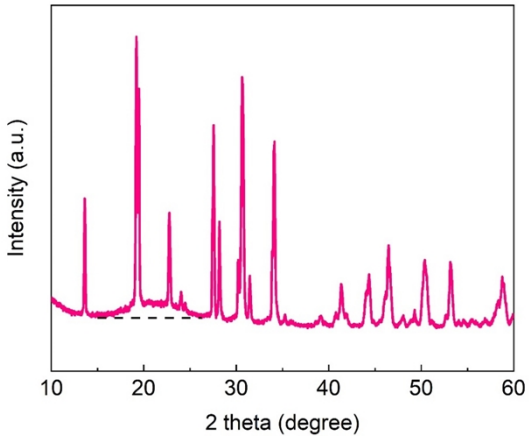

Figure S2. XRD patterns of ISA-NZSP electrolyte.

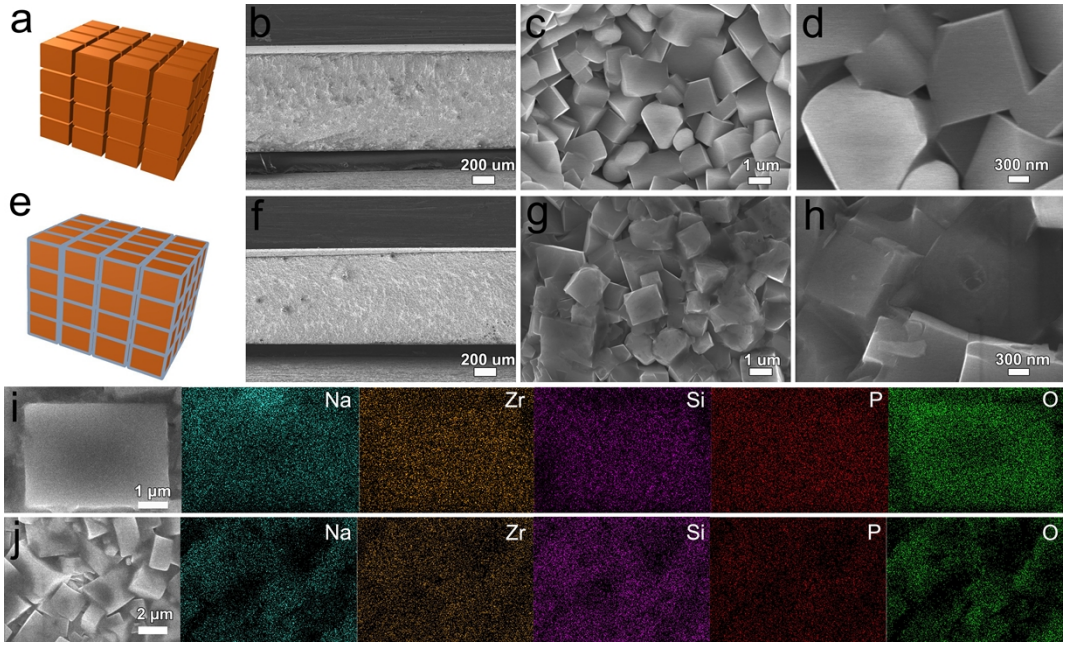

Figure S3. Schematic diagram and Cross-sectional SEM images of (a-d) NZSP and (e-h) ISA-NZSP. (i-j) corresponding EDS mapping of Na, Zr, Si, P and O elements in ISA-NZSP under different magnification.

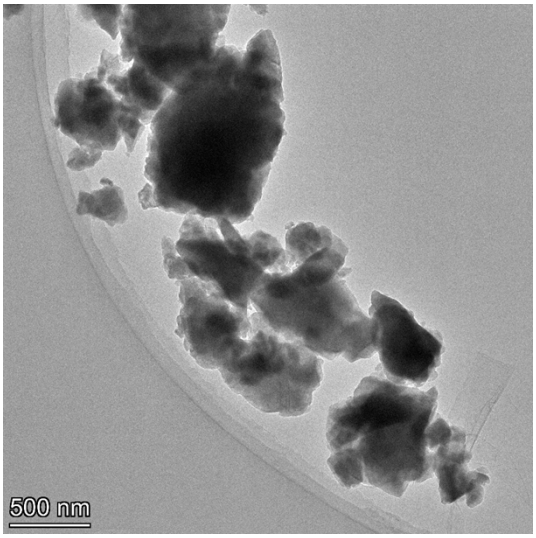

Figure S4. TEM image of ISA-NZSP grind using a mortar and pestle.

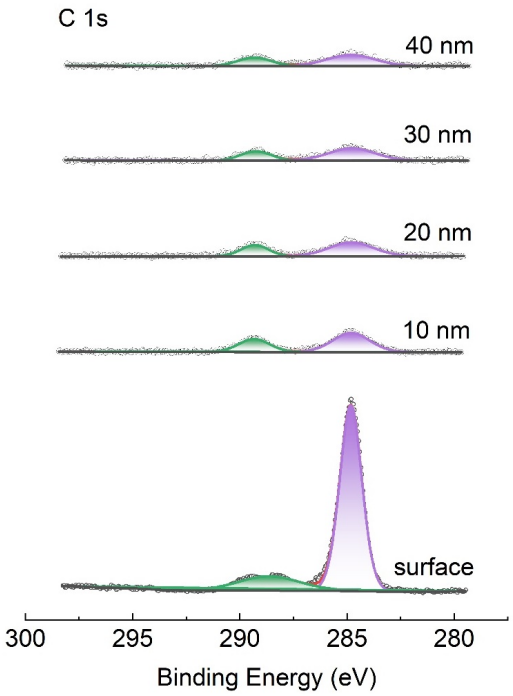

Figure S5. The high-resolution C1s spectra of crystalline NZSP.

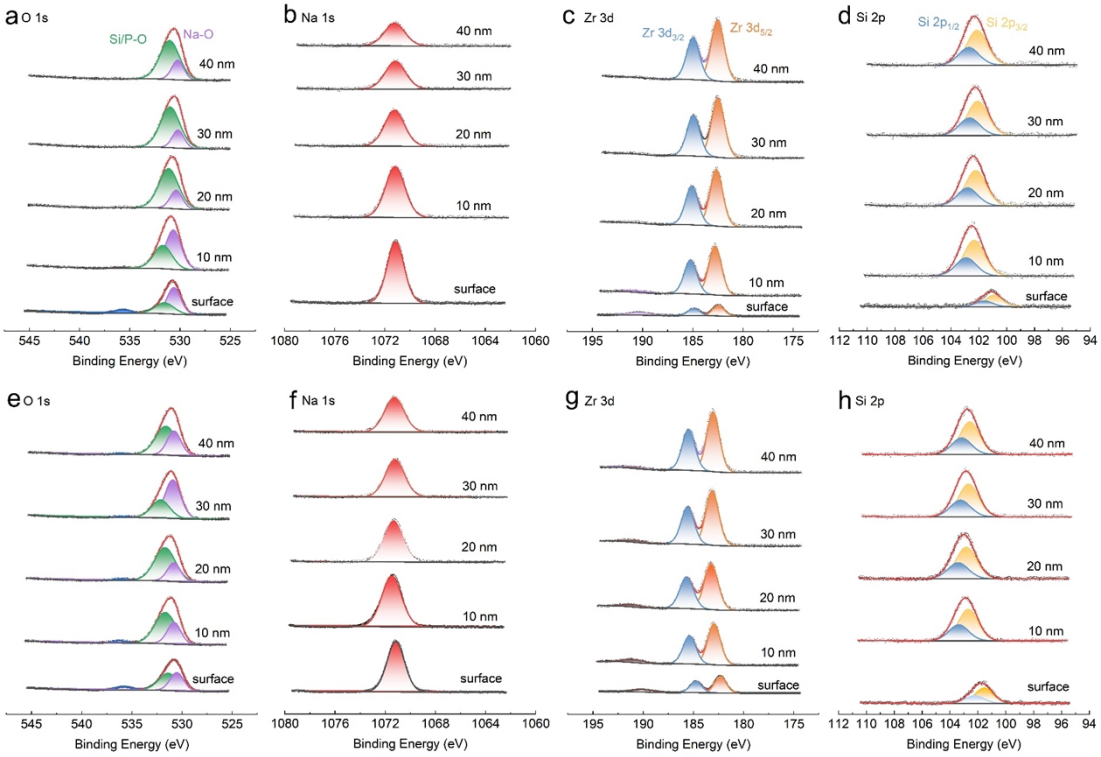

Figure S6. High resolution XPS spectra of surface layer in ISA-NZSP: (a) O1s, (b) Na 1s, (c) Zr 3d, and (d) Si 2p. High resolution XPS spectra of crystalline grains in NZSP: (e) O1s, (f) Na 1s, (g) Zr 3d, and (h) Si 2p.

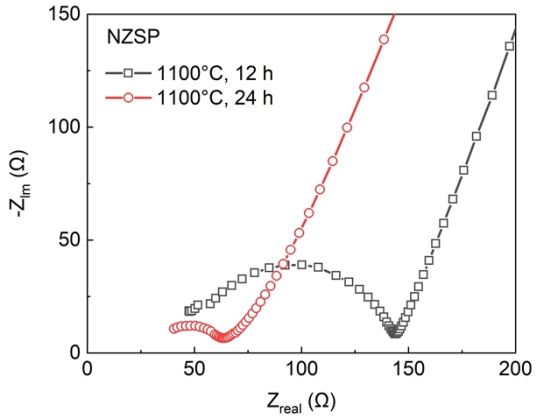

Figure S7. Nyquist plots of NZSP at 1100°C for 12 and 24 h.

Supplementary note: The ionic conductivity is strongly related to the sintering temperature and times. The shrinkage rate varies under different temperature and time, which in turn affects the ionic conductivity. In our study, the measured ionic conductivity of NZSP sintering at 1100°C for 12 h is 0.64 mS cm^{-1}, with a sample diameter of 11.6 mm, which aligns with previous findings (0.61 mS cm^{-1}) [8]. When the sintering time increases to 24 h, the diameter decreases to 11.1 mm with high ionic conductivity of 1.3 mS cm^{-1}. As reported in previous work [9], NZSP sintered at different temperatures ranging from 800 to 1200°C for 10 h exhibited different shrinkage rate, with an optimal ionic conductivity of 1.1 mS cm^{-1}. Unfortunately, quick shrinkage causes sample deformation at 1300°C, rendering NZSP unsuitable for electrolyte application. Thus, we choose an optimal sintering condition of 1250°C for 24h, yielding a dense NZSP electrolyte with ionic conductivity of 2.4 mS cm^{-1}.

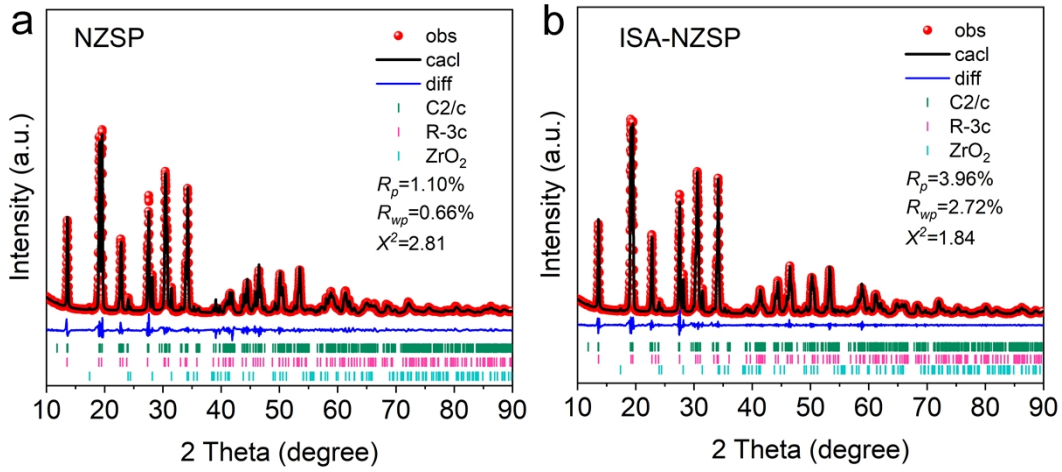

Figure S8. Rietveld refined XRD patterns of a) NZSP and b) ISA-NZSP.

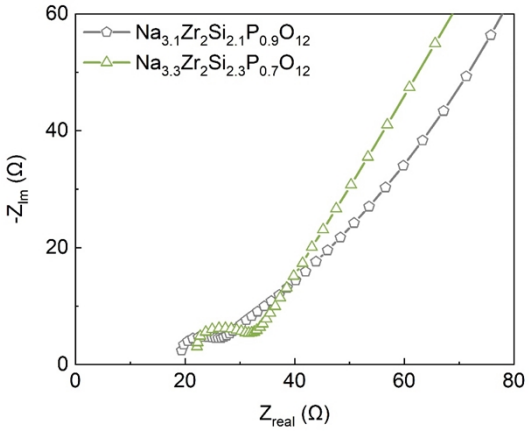

Figure S9. Nyquist plots of $Na_{3.1}Zr_2Si_{2.1}P_{0.9}O_{12}$ and $Na_{3.3}Zr_2Si_{2.3}P_{0.7}O_{12}$ electrolyte pellets.

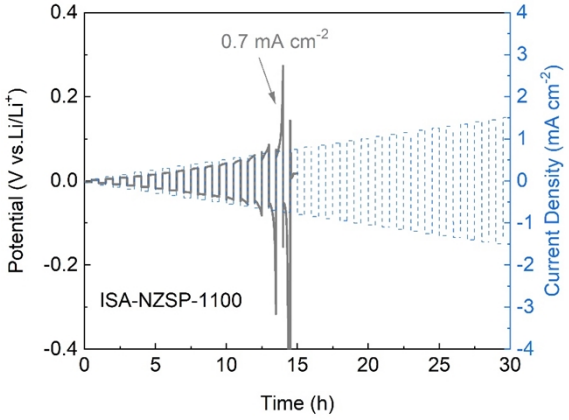

Figure S10. CCD of ISA-NZSP-1100.

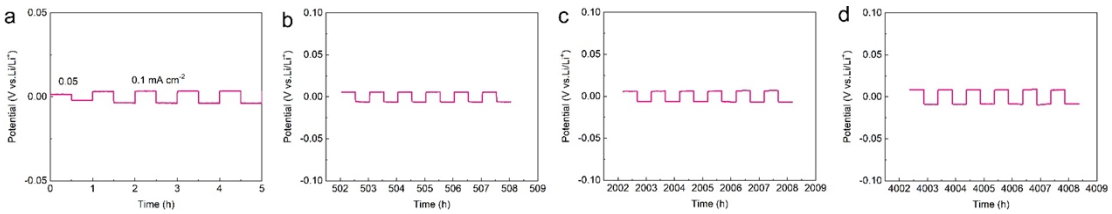

Figure S11. Enlarged galvanostatic cycling of Na/ISA-NZSP/Na batteries at current density of 0.1 mA cm^{-2}.

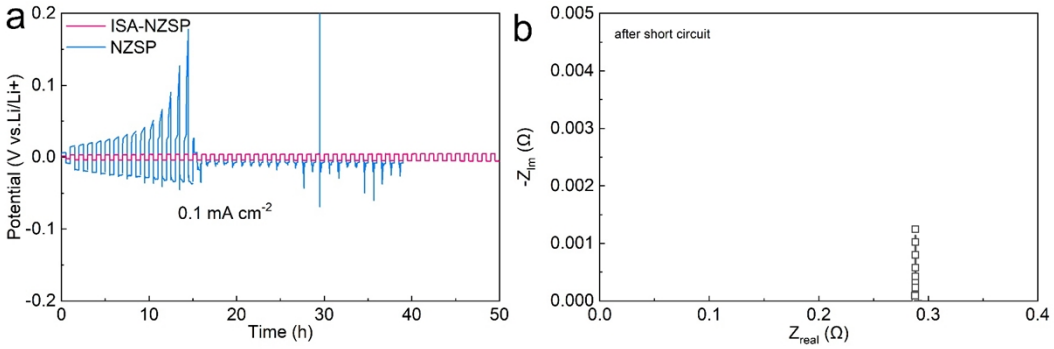

Figure S12. a) Galvanostatic charge/discharge profiles of the Na/SSE/Na symmetric cells during the initial cycling time over 50 h. b) Nyquist plot of Na/SSE/Na symmetric cells after short circuit.

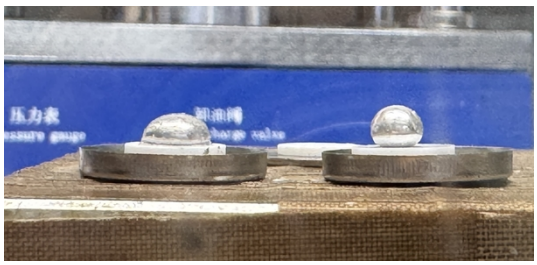

Figure S13. Digital photographs of molten Na on ISA-NZSP (left) and NZSP (right).

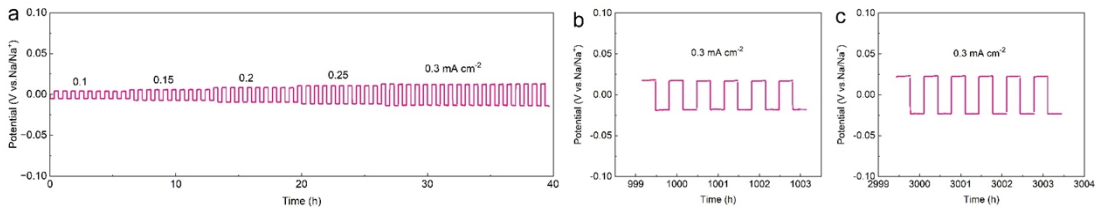

Figure S14. Enlarged galvanostatic cycling of Na/ISA-NZSP/Na batteries at current density of 0.3 mA cm^{-2}.

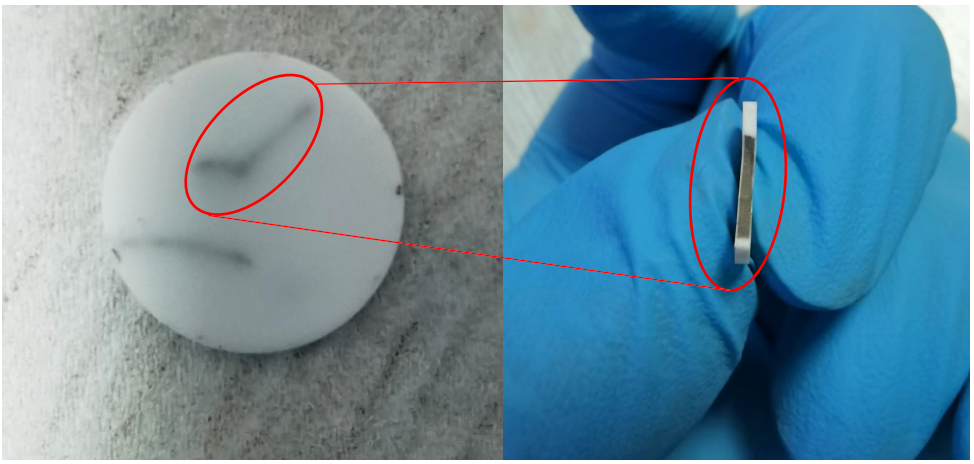

Figure S15. The cross-section digital images of NZSP pellet after short circuiting.

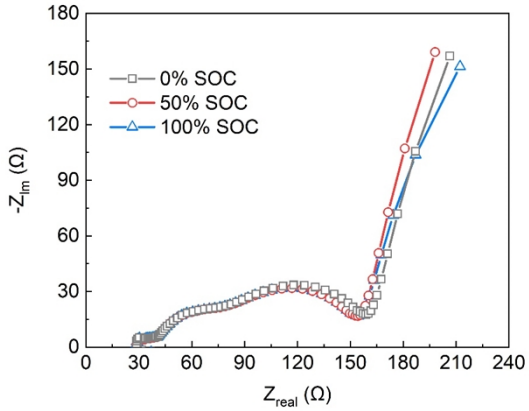

Figure S16. Nyquist plots of Na/ISA-NZSP/$Na_3V_2(PO_4)_3$ battery in different SOC.

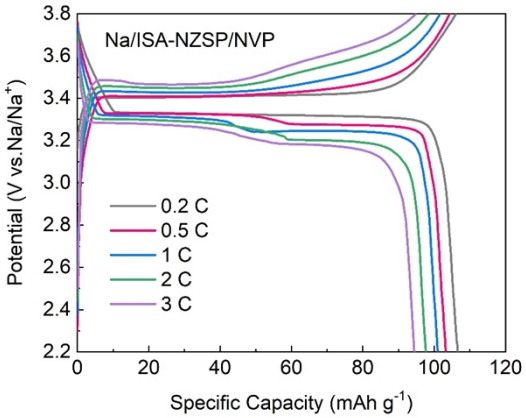

Figure S17. Charge/discharge voltage profiles of Na/ISA-NZSP/NVP at different rates.

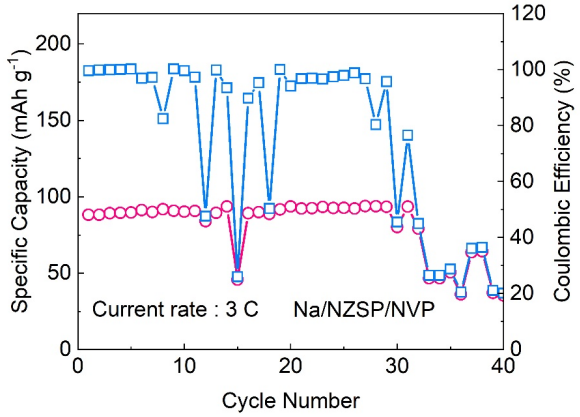

Figure S18. Cycle performance of Na/NZSP/NVP battery at 3 C.

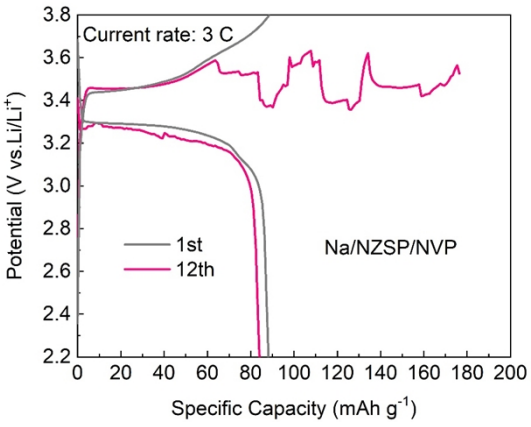

Figure S19. Charge/discharge voltage profiles of Na/ NZSP/NVP battery at 3 C.

Electrolyte	Modification	CCD (mA cm^{-2})	Reference
$Na_{3.4}Zr_{1.8}Cu_{0.2}Si_2PO_{12}$	electrolyte	0.5	Energy Storage Materials 54 (2023) 403–409
$Na_{3.36}Zr_{1.64}Sc_{0.36}Si_2PO_{12}$	electrolyte	0.85	Chem. Mater. 2023, 35, 8686−8694
UW-Na-$Na_3Zr_2Si_2PO_{12}$	electrolyte	0.6	Nat. Commun. 2021, 12 (1), 7109
GBS-$Na_3Zr_2Si_2PO_{12}$	electrolyte	0.55	J. Mater. Chem. A, 2022, 10,5280–5286
$Na_3Zr_2Si_2PO_{12}$-$Na_2B_4O_7$	electrolyte	0.55	Nano Energy 2021, 88, 106293
TiO_2-$Na_3Zr_2Si_2PO_{12}$	electrolyte+ liquid	1.0	Adv. Energy Mater. 2022, 2103607
Pb/C@$Na_3Zr_2Si_2PO_{12}$	interlayer	0.45	Chem. Sci., 2022, 13, 14132–14140
CuO- $Na_3Zr_2Si_2PO_{12}$	interlayer	0.6	Small 2022, 2204487
FeOF-$Na_3Zr_2Si_2PO_{12}$	interlayer	0.6	Adv. Funct. Mater. 2023, 2301670
ZnO-$Na_3Zr_2Si_2PO_{12}$	interlayer	1.1	Adv. Mater. 2023, 2309298
SnF_2-$Na_3Zr_2Si_2PO_{12}$	interlayer	1.8	Adv. Funct. Mater. 2023, 2306558
ZnO-3D $Na_{3.65}Zr_{1.675}Zn_{0.2}Mg_{0.125}Si_2PO_{12}$	electrolyte+ interlayer	40	Energy Environ. Sci., 2024, 17, 727–737

Table S1. Ionic conductivity of various electrolyte.

Electrolyte	σ_b (S cm^{-1})	σ_{gb} (S cm^{-1})	σ_{total} (S cm^{-1})	density
NZSP	4.61	5.14	2.43	90
$Na_{3.1}Zr_2Si_{2.1}P_{0.9}O_{12}$	4.66	15.1	3.56	91
ISA-NZSP	4.63	36.2	4.11	95
$Na_{3.3}Zr_2Si_{2.3}P_{0.7}O_{12}$	3.76	8.22	2.58	90

ISA- $Na_{3.2}Zr_2Si_{2.2}P_{0.8}O_{12}$	electrolyte	1.3	This work

Table S2. Literature review of some CCD value based on NZSP electrolytes.

Table S3. Literature review of some solid-state Na batteries based on NZSP electrolytes.

Electrolyte	T (°C)	Cycle performance	Reference
$Na_{3.3}Zr_{1.7}Lu_{0.3}Si_2PO_{12}$	60	0.1 C /30 cycle /95%	Adv. Energy Mater. 2023, 2301540
SnF_2-$Na_{3.2}Zr_{1.9}Ca_{0.1}Si_2PO_{12}$	30	1 C /300 cycle /80%	Adv. Funct. Mater. 2023, 2306558
$Na_3Zr_2Si_2PO_{12}$-3%NaF	25	0.85 C /200 cycle /91%	Small 2023, 2301230
FeOF-$Na_3Zr_2Si_2PO_{12}$	25	1 C /120 cycle /96%	Adv. Funct. Mater. 2023, 2301670
$Na_3Zr_2Si_2PO_{12}$-10 wt% $Na_2B_4O_7$	25	0.85 C /200 cycle /88%	Nano Energy 2021, 88, 106293
NaBP-$Na_3Hf_2Si_2PO_{12}$	25	1 C /300 cycle /95%	Nano Lett.2022, 22, 13, 5214–5220
TiO_2-$Na_3Zr_2Si_2PO_{12}$	25	0.2 C /100 cycle /86%	Adv. Energy Mater. 2022, 2103607
UW-Na-$Na_3Zr_2Si_2PO_{12}$	25	0.85 C /900 cycle /89%	Nat. Commun. 2021, 12 (1), 7109
Pb/C@$Na_3Zr_2Si_2PO_{12}$	25	0.5 C/200 cycle/79.9%	Chem. Sci., 2022, 13, 14132–14140
Na-TiO_2/ $Na_3Zr_2Si_2PO_{12}$	25	1 C/800 cycles/74.5%	Nano Energy 2024, 122, 109303
SnS_2-$Na_{3.4}Zn_{0.1}Zr_{1.9}Si_{2.2}P_{0.8}O_{12}$	60	1 C/1000 cycles/88.1%	Adv. Funct. Mater. 2024, 2316528
ZnO-3D $Na_{3.65}Zr_{1.675}Zn_{0.2}Mg_{0.125}Si_2PO_{12}$	25	0.2 C/300 cycles/66%	Energy Environ. Sci., 2024, 17, 727–737

ISA- $Na_{3.2}Zr_2Si_{2.2}P_{0.8}O_{12}$	25	3 C /3000 cycles /92%	This work

References

[1] P. Hohenberg, W. Kohn, Phys. Rev. 1964, 136, B864.

[2] W. Kohn, L. J. Sham, Phys. Rev. 1965, 140, A1133.

[3] P. E. Blöchl, Phys. Rev. B 1994, 50, 17953.

[4] G. Kresse, J. Furthmüller, Phys. Rev. B 1996, 54, 11169.

[5] J. P. Perdew, K. Burke, M. Ernzerhof, Phys. Rev. Lett. 1996, 77, 3865.

[6] S. Grimme, J. Antony, S. Ehrlich, H. Krieg, The Journal of Chemical Physics 2010, 132, 154104.

[7] H. J. Monkhorst, J. D. Pack, Phys. Rev. B 1976, 13, 5188.

[8] Zhonghui Gao; Jiayi Yang; Guanchen Li; Thimo Ferber; Junrun Feng; Yuyu Li; Haoyu Fu; Wolfram Jaegermann; Charles W. Monroe; Yunhui Huang, Advanced Energy Materials 2022, 12 (9), 2103607.

[9] Yang Li; Chen Sun; Zheng Sun; Meng Li; Haibo Jin; Yongjie Zhao, Advanced Functional Materials 2024, 2403937.